Paleomagnetic secular variation for a 21,000-year sediment sequence from Cascade Lake, north-central Brooks Range, Arctic Alaska

Douglas P. Steen[1], Joseph S. Stoner[2], Jason P. Briner[3], Darrell S. Kaufman[1]

[1]School of Earth and Sustainability, Northern Arizona University, Flagstaff, Arizona, 86011-4099, USA
5   [2]College of Earth, Ocean, and Atmospheric Sciences, Oregon State University, Corvallis, Oregon, 97331-5503, USA
[3]Department of Geology, University at Buffalo, Buffalo, New York, 14260-1350, USA

Correspondence to: Darrell S. Kaufman (darrell.kaufman@nau.edu)

Abstract. Two > 5-m-long sediment cores from Cascade Lake (68.38° N, 154.60° W), Arctic Alaska, were analyzed to quantify their paleomagnetic properties over the past 21,000 years. Alternating-field demagnetization of the natural remanent
10   magnetization, anhysteretic remanent magnetization, isothermal remanent magnetization, and hysteresis experiments reveal a strong, well-defined characteristic remanent magnetization carried by a low coercivity magnetic component that increases up core. Maximum angular deviation values average < 2°, and average inclination values are within 4° of the geocentric axial dipole prediction. Radiometric ages based on ^{210}Pb and ^{14}C were used to correlate the major inclination features of the resulting paleomagnetic secular variation (PSV) record with those of other regional PSV records, including two geomagnetic field
15   models and the longer series from Burial Lake, located 200 km to the west. Following around 6 ka (cal BP), the ages of PSV fluctuations in Cascade Lake begin to diverge from those of the regional records, reaching a maximum offset of about 2000 years at around 4 ka. Several correlated cryptotephra ages from this section (reported in a companion paper by Davies et al., this volume) support the regional PSV-based chronology and indicate that some of the ^{14}C ages at Cascade Lake are variably too old.

1 Introduction

In paleoclimate and paleo-environmental studies of lake sediments, a firm chronological framework is needed to place observations and corresponding interpretations into regional and global contexts. For Holocene and late Pleistocene lacustrine studies, ^{14}C dating is the most common technique for developing such frameworks. However, dating Quaternary lake sediments in the Arctic using ^{14}C can be problematic due to scarcity of terrestrial macrofossils, and the inheritance of "old carbon" eroded
25   from the surrounding landscape (Gaglioti et al., 2014). Another challenge is the possibility of a hard-water effect, which involves the incorporation of radioactively inert bicarbonate ions into aquatic organisms (e.g., Rea and Colman, 1995; Moore et al., 1998). Researchers in the Arctic and elsewhere have therefore turned to supplementing existing ^{14}C chronologies with additional methods, including paleomagnetic data (e.g., Stoner et al., 2007; Lisé-Pronovost et al., 2009; Barletta et al., 2010; Ólafsdóttir et al., 2013) and tephrochronology (Lowe et al., 2015; Davis et al., this issue).

30   The latest geomagnetic field models provide estimates of site-specific inclination, declination, and field intensity for the past 10 kyr (CALS10k.1b; Korte et al., 2011) and 9 kyr (pfm9k.1b; Nilsson et al., 2014). Although these models are not perfectly constrained for the Alaskan Arctic and they are inherently smoothed both spatially and temporally, their major directional and intensity features can be used for age control by correlation with site-level records (e.g., Barletta et al., 2010). In addition to correlations afforded by field models, individual site-level paleomagnetic records supported by well-constrained
35   geochronological control serve as references for correlated ages based on wiggle matching of prominent fluctuations.

We present a u-channel and hysteresis-based analysis of Cascade Lake, Alaska, paleomagnetic properties and demonstrate that the sediments are suitable for recording directional and relative paleo intensity (RPI) variability since around 21 ka. We then present a PSV-derived age model for Cascade Lake sediments, constructed from correlated age control points using both field

models and an inclination record from Burial Lake, Alaska (Dorfman, 2013). This age model, together with new correlated
40 ages based on cryptotephra identifications (Davies et al., this volume), indicates that our PSV-derived age model provides
improved age control over the ^{14}C data alone.

2 Setting

2.1 Cascade Lake

Cascade Lake (68.38° N, 154.60° W; 990 m asl; Fig. 1) is located on the northern front of the north-central Brooks Range,
45 slightly east and outside of the main Kurupa River valley. The lake has an area of ~ 1 km^2 and reaches a maximum depth of ~
40 m. According to surficial mapping by Hamilton (1980), the Cascade Lake basin was likely glaciated during the Itkillik I
(early Wisconsin) but not during the Itkillik II glaciation (late Wisconsin) (Hamilton, 1982); however, Itkillik II ice likely
entered the drainage of Cascade Lake and may have delivered meltwater to the lake at that time. Cascade Lake presently has
no significant inflow, and the only small outlet flows westward to Kurupa Lake (~ 920 m asl). The small catchment size (~ 10
50 km2) and lack of major inflow likely results in lake deposits dominated by remobilized hillslope sediment derived from till, in
conjunction with variable fluxes of eolian and biogenic sediment.
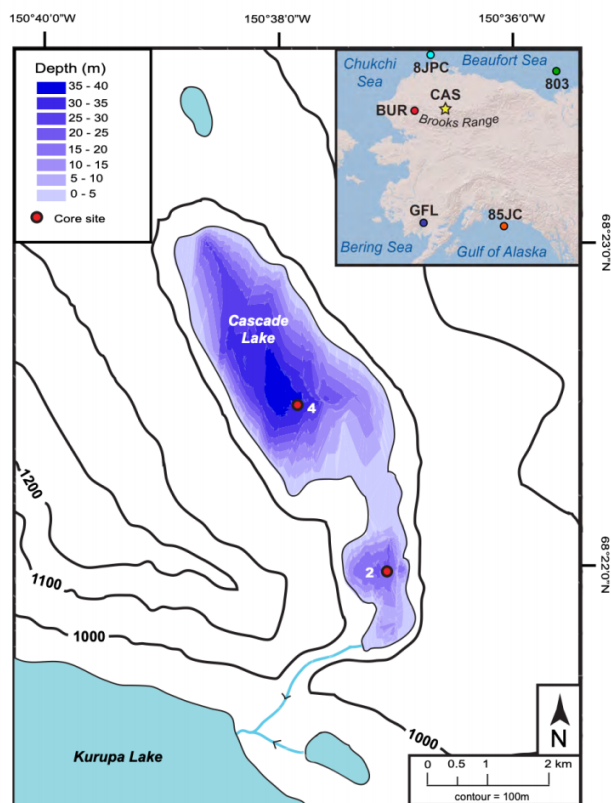
Figure 1: Cascade Lake bathymetry with core sites (2 = CASC-2, 4 = CASC-4). Inset shows the location of Cascade Lake in the north-
55 central Brooks Range, Alaska, along with the locations of previously published paleomagnetic secular variation and relative paleointensity
records used for comparison with this study: Burial Lake (BUR, Dorfman, 2013); Grandfather Lake (GFL, Geiss and Banerjee, 2003); Gulf
of Alaska (85JC, Walczak et al., 2017); Chukchi Sea (8JPC, Lisé-Pronovost et al., 2009); Beaufort Sea (803, Barletta et al., 2008).

2.2 Geomagnetic Setting

60   The relative proximity of Cascade Lake to the magnetic north pole may make the deposits especially sensitive to geomagnetic field variations (Cox, 1970); however, this concept is incompletely tested. Experiments by Aurnou et al. (2003) suggest that fluid movement of "polar vortices" in this region of the outer core may be manifested as geomagnetic field behavior within the "tangent cylinder" (poleward of ~69.5° N and 69.5° S) that is unique to variability outside of the "tangent cylinder" (St-Onge and Stoner, 2011). These potential behaviors of the geomagnetic field are not well understood, however, and recent

65   observations from Svalbard (Ólafsdóttir et al., 2019) suggest mid-latitude geomagnetic dynamics, at least for that part of the polar regions are more likely to apply. Cascade Lake also lies at the edge of the "North American Flux Lobe", one of several regions of concentrated magnetic flux observed from the historical time averaged field (e.g., Bloxham and Gubbins, 1987; Bloxham et al., 1989). Recent research suggests that these flux patches may display oscillatory behavior (Gallet et al., 2009; Stoner et al., 2013), and could be related to heterogeneities in the lower mantle (e.g., Amit et al., 2010; Korte and Holme,

70   2010) that, along with the possible impact of the "tangent cylinder", could result in complex field behaviors in these locations.

3 Methods

3.1 Core recovery and initial analyses

Cascade Lake sediment cores were collected in 2013 using a single-drive (7.7 cm inner-diameter tubing), percussion, piston coring system from the frozen lake surface. Core CASC-4A (5.53 m long) was collected near the depocenter (33.8 m deep) of

75   the primary basin, and CASC-2D (5.41 m long) is from the shallower (18.9 m deep) sub-basin (Fig. 1). An Aquatic Instruments Universal corer was used to recover the surface sediment at each site. Cores were shipped to the National Lacustrine Core Facility, University of Minnesota, where whole cores were scanned with a Geotek MSCL-S fitted with a gamma-ray density sensor to measure wet bulk density (WBD) at 0.5 cm resolution. Cores were then split, described, and imaged using a Geotek Corescan-III line scanner. Magnetic susceptibility and color spectrophotometry were measured using a Bartington point sensor

80   (MS2E) and a Konika Minolta color spectrophotometer, respectively, at 0.5 cm intervals. Additional data available from site CASC-4 include biogenic silica measurements at 5–10 cm intervals and loss-on-ignition (LOI) to determine organic matter (OM) content at 2–5 cm intervals. The analytical methods and further interpretation of these results are provided in Steen (2016).

3.2 Magnetic analyses

85   Sediment cores were sampled for paleomagnetic analysis with rigid plastic 2 x 2 cm u-channels (up to 1 m long), which were taken as close as possible to the center axis of the core, unless either side of a core section appeared less disturbed by minor coring deformation. Low-field magnetic susceptibility (k_{LF}) was measured at 1 cm intervals using an automated u-channel magnetic susceptibility track fitted with a 35 mm Bartington MS loop MS2C metering coil at the Paleo-and-Environmental Magnetism Laboratory (Pmag Lab), Oregon State University. Remanence measurements on u-channels were acquired using a

90   2G Enterprises model 755-1.65UC cryogenic superconducting rock magnetometer equipped with in-line alternating field (AF) demagnetization coils for automated AF demagnetization and measurement and an in-line direct current (DC) coil for anhysteretic remanent magnetization (ARM). An off-line pulse magnetizer was used for imparting an isothermal remanent magnetization (IRM) to the u-channels. Magnetic data processing and visualization was completed using a modified version of the UPmag MATLAB software program (Xuan and Channell, 2009).

95   The natural remanent magnetization (NRM) of u-channels was studied through progressive AF demagnetization of the X, Y, and Z axes and measurement using 16 steps from 10 to 100 mT. Anhysteretic remanent magnetization (ARM) acquisition was performed by imparting a small (0.05 mT) DC field during AF demagnetization on the Z axis, at steps identical to the NRM. The ARM acquired at peak AF of 100 mT was also AF demagnetized at the same steps as the NRM. Isothermal remanent

magnetizations (IRMs) were imparted with the off-line pulse magnetizer using fields of 0.1, 0.3, and 1.0 T, with the latter
100   nominally representing a saturation isothermal remanent magnetization (SIRM). IRMs imparted at 0.1 T were not
demagnetized, and 0.3 T IRMs were AF demagnetized at same 16 steps as the NRM. The SIRMs were demagnetized at three
steps (30, 60, and 100 mT). Due to the response function associated with the pick-up coils of the magnetometer, each
measurement integrates across a ~7 cm interval (Oda and Xuan, 2014). Therefore, the first and last 5 cm from each u-channel
segment are not considered. Additionally, NRM, ARM, ARM acquisition, and IRM were not measured for two short segments
105   (CASC-4A-2a and CASC-2D-2a,13 and 14 cm, respectively).

Because the cores were not azimuthally oriented upon retrieval, declination data were rotated such that each u-channel section
has a mean declination of 0°. This rotation correction is unlikely to be a perfectly accurate representation of declination, but
serves as an objective transformation to meaningfully visualize the declination data. Present declination is ~ 16.5° E at Cascade
Lake, which could be indicative of the magnitude of the expected offsets.

110   Hysteresis experiments on subsampled bulk material were carried out using a Princeton Applied Research Vibrating Sample
Magnetometer (VSM), with the purpose of quantifying changes in magnetic grain size and magnetic mineralogy at the Institute
of Rock Magnetism, University of Minnesota. Saturation magnetization (M_s), saturation remanence (M_{rs}), coercivity (H_c) and
coercivity of remanence H_{cr-dot} calculated from the hysteresis loops themselves (after Fabian and von Dobeneck, 1997) were
derived from hysteresis loops measured to a 1000 mT saturating field and corrected for paramagnetic contributions using the
115   high field slope above 800 mT.

3.3 ^{210}Pb and ^{14}C dating

Core CASC-4B was collected from within 10 m of CASC-4A and the two were correlated by using visual stratigraphy. Core
CASC-4A was sampled for ^{210}Pb analysis at 0.5 cm intervals over the uppermost 10 cm. [210]Pb content was estimated by direct
measurements of [210]Po activity. [226]Ra activity was also analyzed at 10.0–9.5, 6.5–6.0, and 1.5–1.0 cm below lake floor (blf) to
120   determine levels of unsupported ^{210}Pb present in the sediment. A constant-rate-of-supply (CRS) age model (Appleby and
Oldfield, 1978) was applied to allow for changing initial concentrations of unsupported ^{210}Pb with changing sedimentation
rates.

The radiometric-based age model of Cascade Lake was constrained by 11 accelerator mass spectrometry (AMS) ^{14}C dates.
Dated material consisted of various terrestrial plant macrofossils, insect parts, resting eggs, and aquatic vegetation, which were
125   analyzed at the Keck AMS Facility at University of California, Irvine. [14]C dates were calibrated with CALIB 7.1 (Stuiver et
al., 2005) using the IntCal13.14C Northern Hemisphere terrestrial calibration curve (Reimer et al., 2013). AMS ^{14}C dates
obtained from core CASC-4B were combined with CASC-4A dates through visual stratigraphic matching to construct a
composite CASC-4 age model. Calibrated ^{14}C dates are reported as the median of the probability distributions, with 1σ error
ranges. CLAM software for classical age modeling (Blaauw, 2010) was used to fit the calibrated ^{14}C age distributions with a
130   smooth spline with a smoothing parameter of 0.8. The 95% confidence interval from the distribution of 1000 iterations is used
as the uncertainty in the age-depth model.

4 Results and initial interpretations

4.1 General lithologic and magnetic stratigraphy

The sediments recovered in cores from both subbasins of Cascade Lake are undeformed by the coring procedure. The sequence
135   can be separated into three distinct lithologic units based on visual stratigraphy, wet bulk density, organic-matter content, and
variations in magnetic parameters (Fig. 2). Depth intervals for lithologic units are presented for core CASC-4A and magnetic

properties are summarized from the results presented below. Additional sediment descriptions and data are provided by Steen (2016).

L1 (562–393 cm). Lithologic unit 1 (L1) is a pebbly, brown diamicton with a matrix of clay and silt. It contains glacially
140   striated pebbles 1–3 cm in diameter. This section was not sampled using u-channels. There is no clear evidence of an unconformity or depositional hiatus between the diamicton (L1) and the overlying lacustrine unit (L2) in CASC-4A or CASC-2D.

L2 (393–355 cm). Unit 2 (L2) is composed of beige-brown, diffusely to sharply laminated silt and clay that transitions gradationally to grayish-brown silt and clay near the top of the unit. WBD values (1.5–2.0 g cm^{-3}) are significantly lower than
145   in unit L1, and OM steadily increases upward through the unit. Unit L2 exhibits a spike in magnetic parameters relative to unit L3, with k_{LF} exhibiting a low of 4.50 x 10^{-5} at 382 cm to a high of 1.06 x 10^{-4} SI at 361 cm, ARM acquisition at 100 mT AF exhibits a low of 7.89 x 10^{-3} at 381, to a high 2.95 x 10^{-2} A m^{-1} at 363 cm), and IRM$_{0.3T}$ at 0 mT AF exhibits a low of 4.81 x 10^{-1} at 380, to a high 2.03 A m^{-1} at 355 cm) and SIRM at 0 mT AF exhibits a low of 8.97 x 10^{-1} at 380, to a high 2.35 A m^{-1} at 355 cm. (Fig. 2). A ~5-cm-thick interval of olive-green to gray, faintly laminated sediment near the top of unit L2 in CASC-
150   2D is visually similar to unit L3. This distinctly colored interval corresponds with high intensities in all parameters that are slightly offset in depth suggesting a complex magnetic mineralogic suite that hint at the authogenic creation of greigite, but without further analysis are beyond the scope of this manuscript to identify.

L3 (355–0 cm). Unit 3 consists of irregular, millimeter- to centimeter-scale bands of olive-green, greenish-gray, and brown silt and clay. Unit L3 is similar in thickness in the two cores (311 to 0 cm in CASC-2D). Magnetic properties are in general more
155   variable in the lower part of the unit, becoming more consistent up core. k_{LF} is, however, somewhat different and similarly variable throughout, decreasing from highs around 5.5 x 10^{-5} SI at the base of the unit to around 3 x 10^{-5} SI at the top. ARM$_{aq}$ at 100 mT are generally lower 1.8 x 10^{-2} and variable (1σ = 4.2 x 10^{-3} A m^{-1}) below 220 cm and higher ~2.8 x 10^{-2} and variable (1σ = 4 x 10^{-3} A m^{-1}) above, with a high value of 3.82 x 10^{-2} A m^{-1} at 157 cm. IRM$_{0.3T}$ at 0 mT AF are less variable with mean values of 0.56 A m^{-1} and 1σ of 0.11 A m^{-1}. SIRM at 0 mT AF are slightly higher with a mean 0.7 A m^{-1} and 1σ of 0.12 A m^{-1}.

160   Core CASC-2D displays a dark, highly magnetic layer (IRM$_{0.3T}$ = 9.26 A m^{-1}; 307 cm blf) that forms a sharp contact with laminated sediments below, but grades diffusely into laminated sediments above. Immediately up-core of this interval, IRM$_{0.3T}$ does not cleanly decrease in intensity with higher AF suggesting that the SQUID electronics are unable to keep up with the change in counts resulting in artifacts within the subsequent magnetic measurements. This is a common problem associated with overly strong samples that persists even after several AF demagnetization steps. Therefore, IRM$_{0.3T}$ data from ~300–251
165   cm blf in CASC-2D are disregarded (shown shaded in Fig. 2), and SIRM for the u-channel section (387-251 cm blf) was not measured.
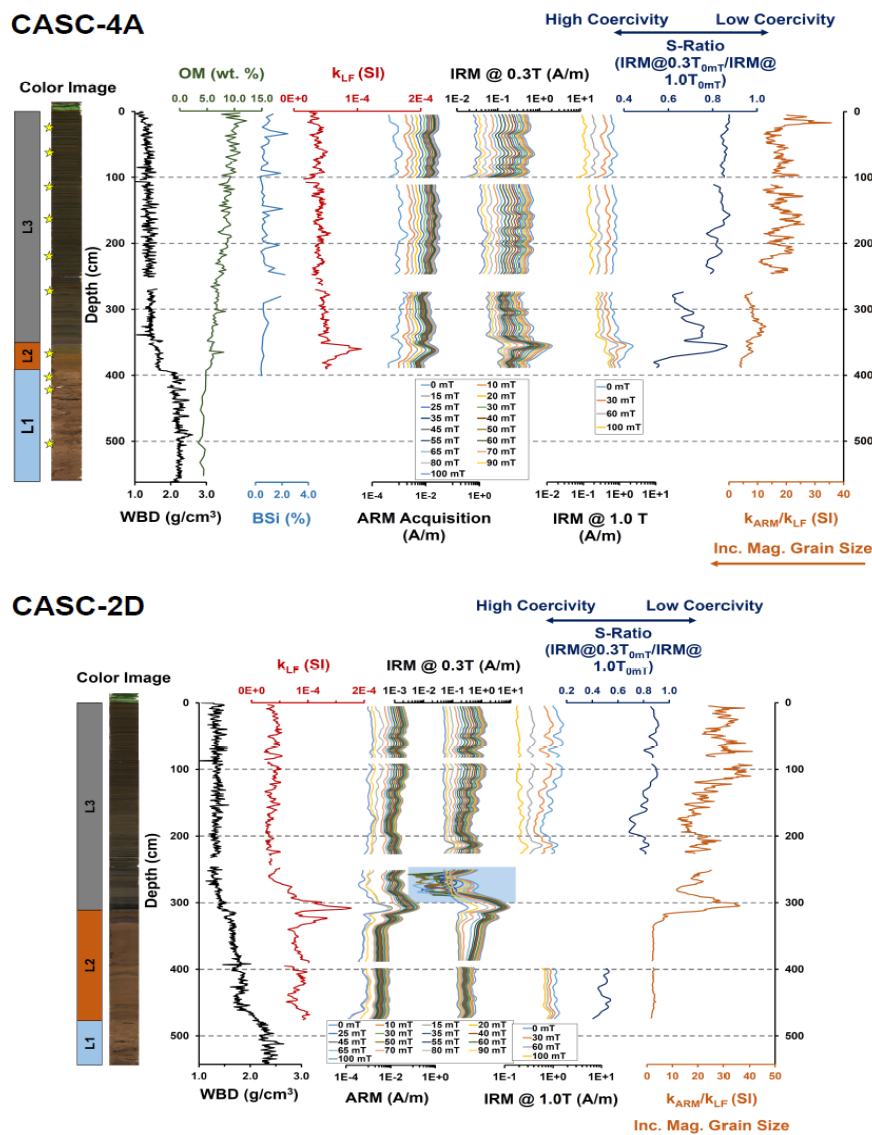
Figure 2: Cascade Lake wet bulk density (WBD), organic matter (OM), biogenic silica (BSi), low-field magnetic susceptibility (k_{LF}), anhysteretic remanent magnetization (ARM), and isothermal remanent magnetization (IRM) plotted by depth for cores CASC-4A and CASC-2D. Also plotted are S-ratio (magnetic mineralogy proxy) and anhysteretic susceptibility (k_{ARM})/k_{LF} (magnetic grain size proxy). Linescan images and lithologic unit (L1-L3) at left. Yellow stars indicate the depths of hysteresis samples.

4.2 S-ratios and k_{ARM}/k_{LF}

Cascade Lake S-ratios display an overall increasing trend up-core (Fig. 2). CASC-4A contains an S-ratio peak at ~ 356 cm, at the transition from L2 to L3. This peak is not visible in CASC-2D, due to complications in measuring IRM at 0.3 T and 1.0 T in the u-channel section containing the L2–L3 transition. S-ratios vary between 0.40–0.92 in Cascade Lake sediment, with an increasing up-core trend indicating an increasing proportion of low-coercivity magnetic material, an interpretation supported by the up-core increase in ARM (Fig. 2).

180   Cascade Lake k_{ARM}/k_{LF} and $k_{ARM}/SIRM$ (Steen, 2016) and ratios also show an increasing trend, and reach a clear minimum in L2 (Fig. 2). Assuming these are mostly driven by the ferrimagnetic assemblage, these ratios suggest a coarser magnetic grain size in L2 compared to L3, and generally decreasing up-core magnetic grain sizes in L3 consistent with the progressive addition of a separate fine-grained ferrimagnetic component to the magnetic assemblage.

4.3 Hysteresis, magnetic grain size and mineralogy

185   Hysteresis experiments were performed on ten representative samples from the three units in core CASC-4A. After slope correction for paramagnetic contributions, data from the three units exhibit distinct hysteresis loops and positions on conventional plots (cf., Day et al., 1977; Wang and Van der Voo, 2004) (Fig. 3). However, the grain-size boundaries depicted are only a useful approximation as the proportion of high-coercivity materials, especially in L3 and possibly L2, are not directly applicable to a Day plot. Unit L1 hysteresis loops are characterized by high coercivities and a subtle "wasp-waisted" shape

190   (Roberts et al., 1995; Tauxe et al., 1996); the data plot to the far right on a Day diagram, suggesting a significant antiferromagnetic (e.g., hematite, goethite) contribution, with a fine ferrimagnetic component (Roberts et al., 2018). Unit L2 hysteresis loops are also "wasp-waisted", with an apparent antiferromagnetic and perhaps coarser ferrimagnetic contributions (Roberts et al., 2018). Unit L3 data are consistent with fine ferrimagnetic material, approaching single-domain threshold on a Day diagram on top of substantial concentration.
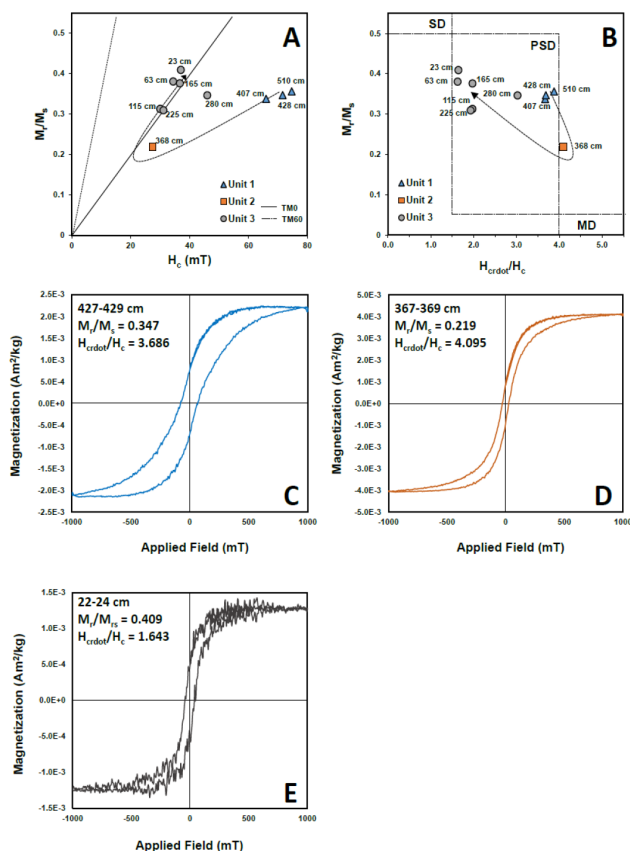
Figure 3: Hysteresis data for samples from core CASC-4A. (A) Saturation remanence (M_r)/saturation magnetization (M_s) versus coercivity (H_c) (after Wang and Van der Woo, 2004) showing typical lines for Ti-rich (TM-60) and Ti-poor (TM-0) titanomagnetite; (B) Day plot of hysteresis data, an approximation of magnetic domain state for pure magnetite samples (after Day et al., 1977). Typical hysteresis loops are plotted for samples from (C) Unit L1, (D) Unit L2, and (E) Unit L3. Note that hysteresis loops are plotted on different magnetization scales.

200   Dotted lines in (A) and (B) show general up-core trends.

Samples from L1 and L3 plot within the pseudo-single domain (PSD) range (~0.1–10 μm for Ti-poor magnetite) on a typical Day plot (Day et al., 1977), while the L2 sample falls just outside of this boundary (Fig. 3b). High M_r/M_s values for L3 samples (Fig. 3a,b,e) suggest the presence of very fine PSD, or even SD, magnetite within this unit (Roberts et al., 1995). Hysteresis
205 measurements indicate that L2 (Fig. 3d) may incorporate significant amounts of both ferrimagnetic and antiferromagnetic material, while L1 (Fig. 3c) is likely dominated by high-coercivity material (e.g., hematite) and a smaller proportion of PSD magnetite (Roberts et al., 1995).

The k_{ARM} vs. k_{LF} calibration of King et al. (1982) also suggests extremely fined grain magnetic grain sizes of < 0.1 μm for L3, and somewhat coarser L2 magnetic grain sizes of < 5 μm (Fig. 4). While this relationship likely accurately represents the
210 relative magnetic grain size relationship between L2 and L3, these plots should not be interpreted as absolute grain size estimates. However, due to the increased influence of high coercivity material (hematite) on the SIRM and hysteresis data, this relationship (k_{ARM}/k_{LF}) may be a more realistic indicator of relative magnetite grain size at Cascade Lake.
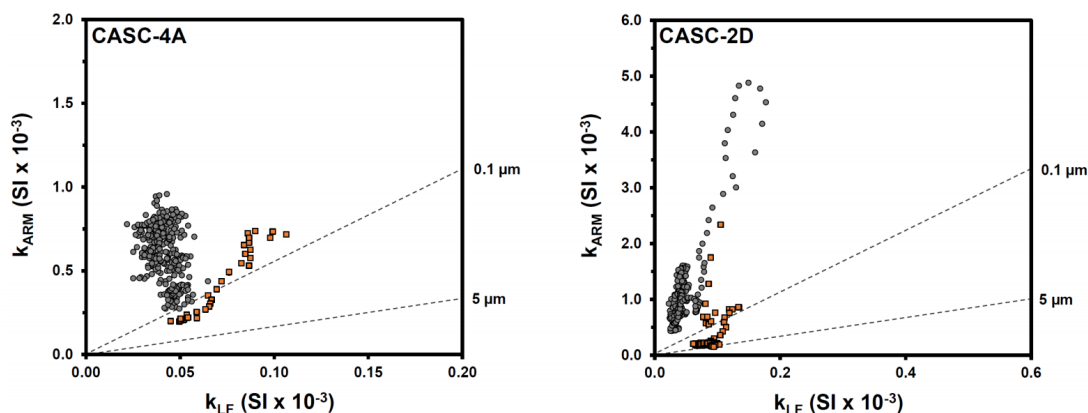
215 **Figure 4.** Low-field susceptibility (k_{LF}) vs. anhysteretic susceptibility (k_{ARM}) as a magnetite grain-size indicator, based on the calibration of King et al. (1982) for samples of dispersed (~ 1% by volume) equidimensional magnetite grains. Dashed lines are empirically derived characteristic grain sizes. L2 (orange squares) and L3 (gray circles) are plotted separately to discern lithologically-separate differences in magnetic grain size. L1 (glacial till) is not included because that interval was not sampled with u-channels.

4.4 Characteristic remanent magnetization

220 Cascade Lake sediments carry a generally strong, stable, and well-defined NRM signal (Fig. 5). Component inclination and declination were calculated using Principal Component Analysis (PCA; Kirschvink, 1980) from the UPmag software (Xuan and Channell, 2009) over the 20–70 mT (11 steps) AF demagnetization range after removal of a low coercivity viscous remanent magnetization intermittently observed throughout the u-channels (Fig. 6). Maximum angular deviation (MAD) values in unit L3 average 0.56° for CASC-4A and 0.77° for CASC-2D, indicating a remarkably stable magnetization defining
225 the ChRM. MAD values are slightly higher in unit L2, averaging 0.84° and 3.70° for CASC-4A and CASC-2D, respectively. NRM_{30mT}/NRM_{0mT} values range from 0.61–0.87 throughout CASC-4A, suggesting a consistently hard NRM held by a high-coercivity ferrimagnetic component (Fig. 3), consistent with the hysteresis and k_{ARM} vs. k_{LF} observations. Average MAD values fall well within the recommendation of Stoner and St-Onge (2007) of < 5° for high-quality PSV and RPI studies, and individual MAD values > 5° only occur from 387–379 cm on either side of section break and in the lower 10 cm of CASC-2D
230 (Fig. 5). These intervals are not considered in our paleomagnetic reconstructions. ChRM average inclinations for CASC-4A

(80.5°) and CASC-2D (74.8°) are close to, and for much of each record, they vary around the predicted geocentric axial dipole (GAD) inclination for Cascade Lake (78.8°), indicating that these sediments are reliable recorders of geomagnetic direction.
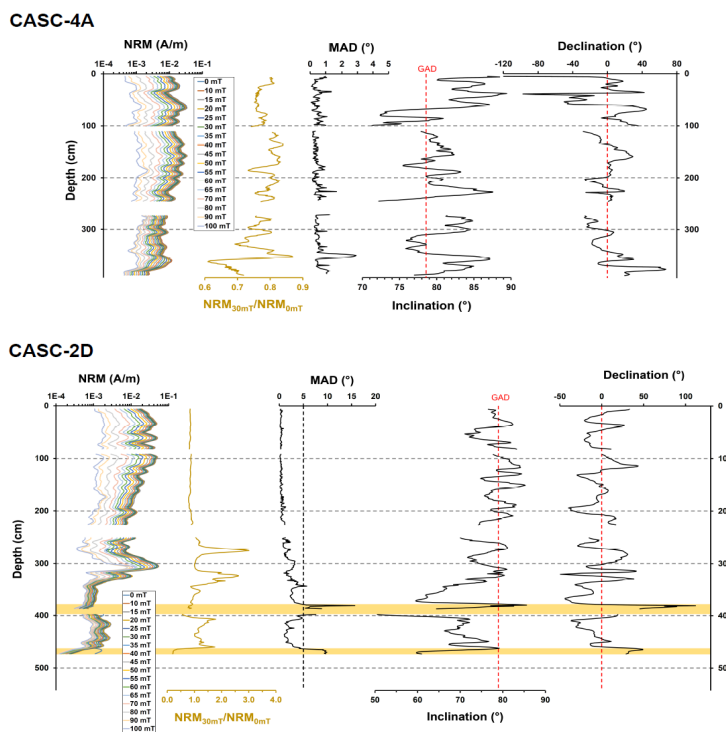
Figure 5: Cascade Lake natural remanent magnetization (NRM), NRM coercivity, maximum angular deviation (MAD) values, inclination,
235 and declination vs. depth for CASC-4A (top) and CASC-2D (bottom). The dashed red lines indicate the expected geocentric axial dipole (GAD) inclination for Cascade Lake (78.8°). Yellow bars indicate intervals with MAD values greater than 5°. Because core sections are not azimuthally oriented, and because each section is oriented differently, the declination record of each u-channel section has been rotated to a mean of 0°.
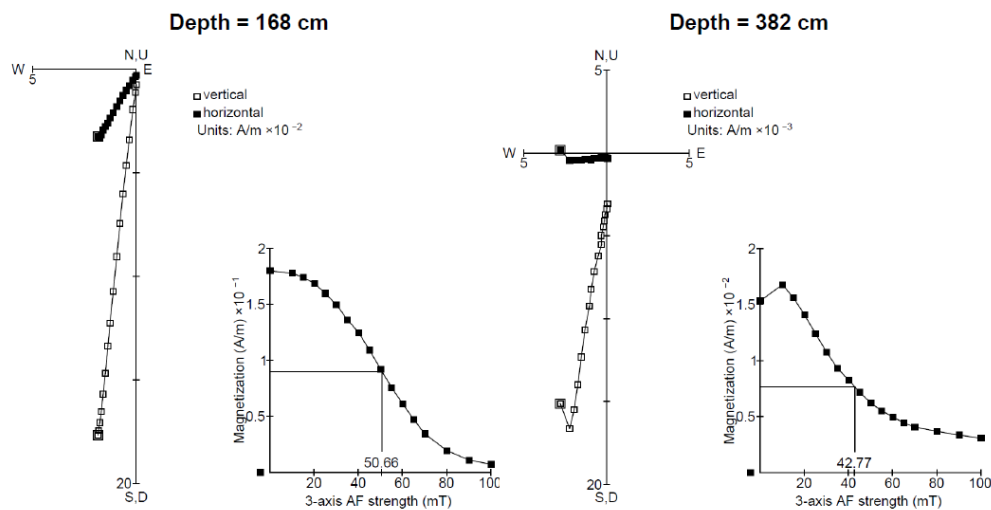
240 **Figure 6:** Typical orthogonal projections and demagnetization behavior of the natural remanent magnetization (NRM) at selected depths in the composite 4A-2D record (168 cm from L3; 382 cm from L2). Median destructive fields (MDFs) of the NRM are shown on demagnetization plots. Plots created using PuffinPlot (Lurcock and Wilson, 2012).

4.5 Normalized remanence (relative paleointensity)

To assess whether these sediments record variations in geomagnetic field strength, we explore three commonly used
245 normalization approaches over the stable ChRM demagnetization range ($NRM_{20–70\ mT}$). First, NRM at the 30, 45, and 60 mT
demagnetization steps was normalized using k_{LF} (NRM/k_{LF}). Second, the slope of the NRM at demagnetization ranges 20–50,
20–70, and 40–70 mT was normalized using the slope of the ARM at the same demagnetization steps (NRM_{X-YmT}/ARM_{X-YmT}).
Third, the slope of the NRM at the three demagnetization ranges listed above was normalized using the slope of the IRM at
the same demagnetization steps (NRM_{X-YmT}/IRM_{X-YmT}). This "slope method" (e.g., Channell et al., 2002) offers the advantage
250 of normalization using a broad NRM demagnetization range, rather than relying on a single demagnetization step.

All three normalization methods (NRM/k_{LF}, NRM/ARM, NRM/IRM) produce broadly similar results in the shape of the
normalized remanence curves regardless of the coercivity window chosen (Fig. 7a). This consistency suggests that reliable
relative paleointensity is likely preserved; however, $NRM_{20-70mT}/ARM_{20-70mT}$ does resemble its normalizer. Comparisons of
$NRM_{20-70mT}/ARM_{20-70mT}$ vs. ARM_{45mT} display moderate positive correlations in both unit L2 ($R^2 = 0.38$; Fig. 7f) and unit L3
255 ($R^2 = 0.45$; Fig. 7c), suggesting that lithologic variability may not be adequately removed from the normalized intensity record.
In contrast, NRM/k_{LF} (Fig. 7b, e) and NRM/IRM (Fig. 7d, g) bear little resemblance to their respective normalizers (k_{LF} and
IRM_{45mT}, respectively), while showing a very similar normalized remanence pattern to NRM/ARM. NRM_{45mT}/k_{LF} displays a
negative correlation ($R^2 = 0.29$) in L3 and no correlation in L2 ($R^2 = 0.04$). $NRM_{20-70mT}/IRM_{20-70mT}$ shows no correlation with
IRM_{45mT} in L2 or L3 ($R^2 = 0.04$ and 0.01, respectively; Fig. 7d, g).

4.6 Composite paleomagnetic record

Due to the missing upper sediment, shallower coring depth, increased lithologic variability and higher MAD values in CASC-
2D, we focus instead on CASC-4A as the main paleomagnetic record from Cascade Lake. However, CASC-2D contains a
thicker version of unit L2. To create a more detailed composite sequence, the data from unit L2 in core CASC-2D were spliced
onto the entirety of the paleomagnetic data from core CASC-4A by matching their inclination records. The data from 473–343
265 cm blf from CASC-2D were used to extend the paleomagnetic record downward to a composite depth of 520 cm blf,
specifically by setting 389 cm depth in CASC-4A equal to 343 cm depth in CASC-D2. This match is supported by the transition
from units L2 to L3 in each core, which agrees with the inclination match. The match also suggests that the CASC-2D
paleomagnetic record is missing > 40 cm of sediment at the top of the sequence when compared to CASC-4A. The resulting
composite sequence (CASC-4A-2D) therefore comprises the quality and completeness of CASC-4A for the upper 389 cm,
270 plus the data from the expanded L2 section in CASC-2D over the lower 131 cm. This composite L2-L3 sequence is underlain
by glacial diamicton (L1) in both cores, which was not analyzed for continuous magnetic properties.
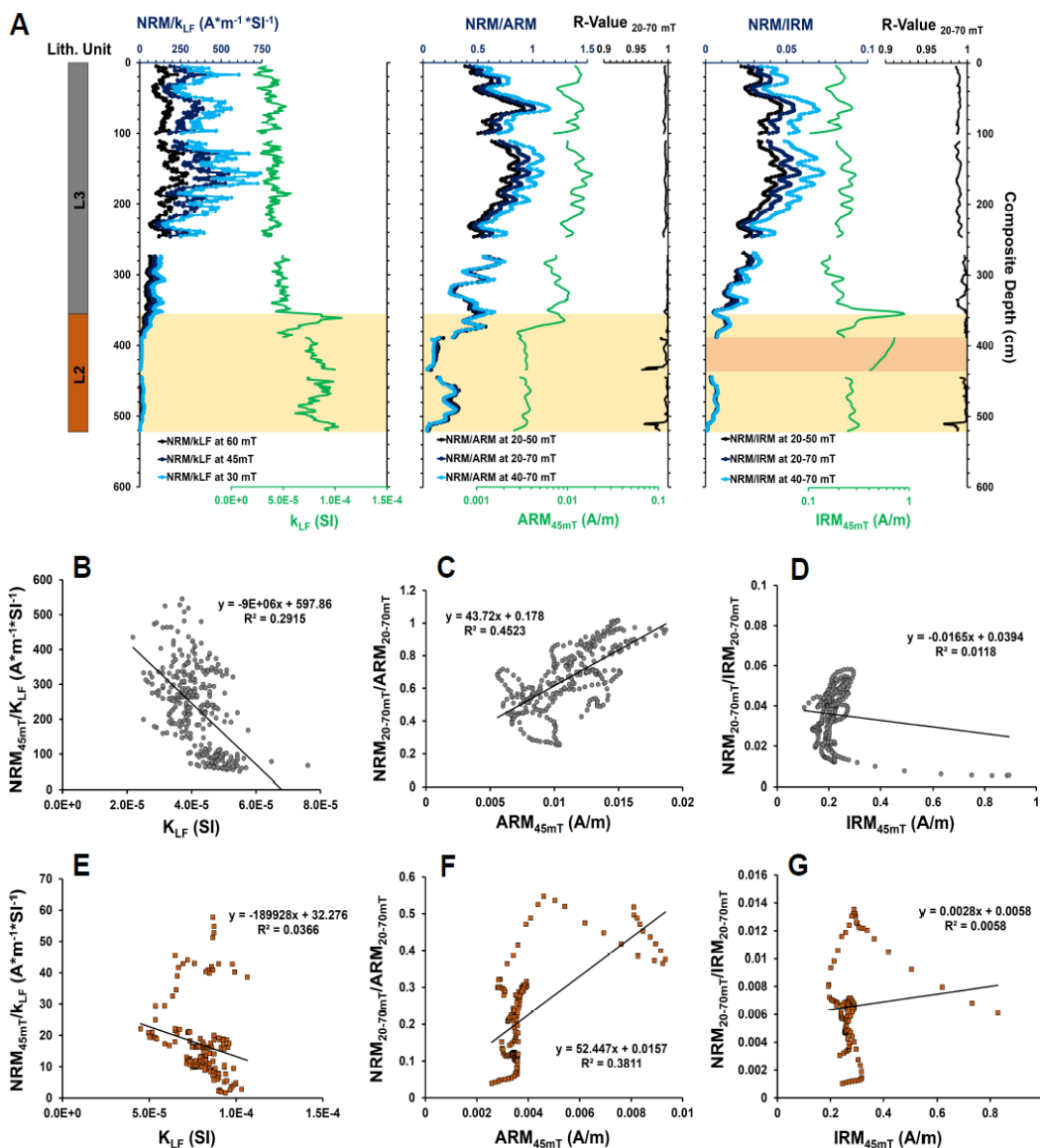
Figure 7: (**A**) Three methods for estimating relative paleointensity (RPI) of Cascade Lake sediment: (1) NRM/k_{LF} at the 30, 45, and 60 mT AF demagnetization steps; (2) NRM/ARM using the 20–50, 20–70, and 40–70 mT demagnetization ranges; (3) NRM/IRM using the 20–50, 20–70 and 40–70 mT demagnetization ranges, plotted alongside respective normalizers and R-values based on least squares linear regression. R-values are a measure of the quality of the "slope method" approximation, and represent the correlation between the NRM and the normalizer (ARM or IRM) over the selected demagnetization range. Lightly shaded region indicates relative paleointensity (RPI) estimates for unit L2, which should be treated with caution due to lithologic contrast with unit L3. Dark shaded region indicates an interval of rapidly changing IRM values, where RPI estimation is likely not feasible. (**B-D**) Normalized remanence values vs. respective normalizers within unit L3. (**E-G**) Same as in (B-D), but for unit L2.

4.7 Radiometric age model

285 Based on CRS modeling of ^{210}Pb data (Table 1) (Appleby and Oldfield, 1978), the uppermost 3.6 cm of sediment from site CASC-4 was likely deposited within the last ~140 years (Fig. 8). Uncertainty in the CRS age model was estimated by first-order propagation of counting error after Binford (1990), yielding an age range of 150–135 years (95% C.I.) at 3.6 cm blf. This depth is interpreted as the limit of meaningful age estimation by ^{210}Pb dating, and suggests sedimentation rates of 24–27 cm kyr^{-1} in the uppermost portion of CASC-4A.

290 The ^{210}Pb age profile was combined with ^{14}C dates (Table 2) to generate a provisional age-depth model for site CASC-4 (Fig. 8). Two ^{14}C dates (UCIAMS 134422, 128096) were rejected as outliers; both are anomalously old relative to the down-core trend of the surrounding ^{14}C dates. On the basis of this age model, the average sedimentation rate is 23.7 cm kyr^{-1}, as evaluated to the deepest ^{14}C age at 351 cm blf. The extrapolated age of the unit L2-L3 boundary at 355 cm is estimated at 15.2 ka (15.6–14.1 ka, 95% C.I.). The average 95% confidence interval over the entire radiometric age model is ± 345 years.

Table 1. Cascade Lake site CASC-4 ^{210}Pb dates.

CASC-4A depth blf (cm)	Total ^{210}Po activity (DPM g^{-1})	Unsupported ^{210}Po activity (DPM g^{-1})	Age at bottom of interval (yr)	2σ error (± yr)
0–0.5	8.36	6.96	23	1
0.5–1.0	5.25	3.85	48	1
1.0 –1.5	2.92	1.52	67	2
1.5–2.25	2.13	0.73	83	2
2.25–3.0	2.05	0.65	112	4
3.0–3.6	1.73	0.33	143	7

295
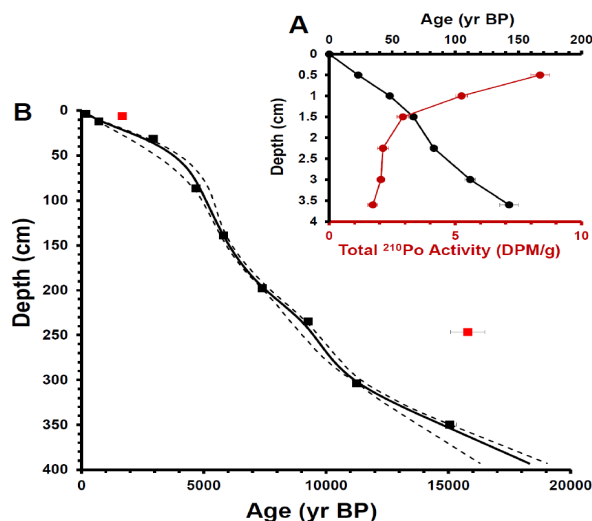
Figure 8: Cascade Lake radiometric age-depth model. (**A**) ^{210}Pb activity inferred using ^{210}Po activity counts, reported in disintegrations per minute per gram of sediment (DPM g^{-1}) (Table 1). The constant-rate-of-supply (CRS) model was used for ^{210}Pb age-depth modeling (after
300 Appleby and Oldfield, 1978), and error (2σ) at the bottom of each sampled interval was calculated using a first-order propagation of error technique (Binford, 1990). (**B**) ^{14}C dates (Table 2) were fit with a smooth spline with a "smoothing parameter" of 0.8 using CLAM software (Blaauw, 2010). Rejected dates are shown in red. Dotted lines define the 95% confidence interval for the CLAM age model.

Table 2. Cascade Lake site CASC-4 ^{14}C dates.

Sample ID (UCIAMS)	Depth blf (cm)	^{14}C age (yr BP)	Error (± yr)	Median cal. age (yr BP)	1σ range (± yr)	Material
147384#	2.6–4.6	170	30	180	140	Resting eggs, mixed aquatic fragments
134422*	5.5–7.5	1765	20	1663	40	Insects, twigs, leaves, bryophyte, eggs
147383#	11–13	785	45	712	30	Leaf fragments, resting eggs, mixed aquatic fragments
131742	30.5–32.5	2825	25	2926	40	Insects, moss fragments, resting eggs, fine unidentified pieces
128095	85.75–87.75	4160	120	4680	150	Insects, twigs, leaves, bryophyte, resting eggs
131743	138–140	5085	20	5808	70	Insects, moss fragments, resting eggs, fine unidentified pieces
131744	197–199	6485	25	7392	50	Insects, moss fragments, resting eggs, fine unidentified pieces
134423	233.5–235.5	8270	35	9269	130	Insects, twigs, leaves, resting eggs, fine unidentified pieces
128096*	245–248	13200	450	15797	695	Insects, aquatic vegetation, twigs, resting eggs
131745	303–304	9875	35	11264	30	Insects, moss fragments, resting eggs, fine unidentified pieces
137726	348.5–351	12690	150	15046	295	Insects, twig, leaf fragments

* ^{14}C dates rejected as outliers.
\# ^{14}C dates from surface core CASC-4B. All other dates are from CASC-4A.

5 Discussion

5.1 Magnetic assemblage

305 Hysteresis experiments, remanence measurements and ratios (S-ratios, k_{ARM}/k_{LF}) document an up-core transition (L1 to L3) from a magnetic assemblage dominated by high coercivity, likely antiferromagnetic (e.g., hematite) minerals as demonstrated by S-ratios, to one where very fine-grained ferrimagnetic (e.g., (titano)magnetite) components are a much more important part of the assemblage, although high-coercivity components are still present. This transition reflects the deglacial and

310 environmental evolution of the catchment, with unit L1 comprising minerogenic sediment glacially sourced from local bedrock. In contrast, unit L3 is magnetically dominated by low-coercivity magnetic material (e.g., (titano)magnetite), but also incorporates a subordinate amount of high-coercivity material.

5.2 Development of PSV age model

Assuming the inclination changes recorded in Cascade Lake sediment accurately reflect the timing and variations of Earth's

315 magnetic field, comparisons with other inclination records can be used for stratigraphic correlations, and for geochronological purposes when well-dated records are available. Due to the possibility of relatively localized geomagnetic field behavior, we focus our comparisons with existing regional records mainly on Burial Lake (Dorfman, 2013), the one closest to our study site in the north-central Brooks Range. We visually matched prominent features (tie points) in the Cascade Lake inclination record to geomagnetic field models and the Burial Lake paleomagnetic record. The field models used for the inclination comparisons

320 are CALS10k.1b (Korte et al., 2011) and pfm9k.1b (Nilsson et al., 2014); both provide inclination, declination, and field intensity predictions for any given site coordinates over the specified time interval. The CALS10k.1b model incorporates archeomagnetic data from the GEOMAGIA50 database (Donadini et al., 2006; Korhonen et al., 2008) as well as 75 selected sedimentary paleomagnetic records from the SED12k data compilation (Donadini et al., 2009; Korte et al., 2011). The pfm9k.1b model uses a dataset similar to that of Korte et al. (2011), but excludes sedimentary sequences dated by using ^{14}C

325 on bulk sediment, archeomagnetic data with large temporal uncertainties, and some records with paleomagnetic behavior incompatible with the majority of others. Both field models have an estimated temporal resolution of around ± 500 years, based on sediment age uncertainties and bootstrap sampling (Korte et al., 2011) as well as comparisons of model power spectra at different coordinates (Nilsson et al., 2014). The Burial Lake ^{14}C age model is likely more reliable than the Cascade Lake ^{14}C age model because Burial Lake ^{14}C samples only include terrestrial macrofossils (decreasing the likelihood of a hard-water

330 or reworked old carbon effects) and because the sedimentation rate at Burial Lake is rather linear over the past ~ 17 kyr (Dorfman, 2013; Dorfman et al., 2015; Finkenbinder et al., 2015). We adopted the published 95% confidence intervals from the published ^{14}C age model for the age uncertainty of the age-control points.

We developed two alternative PSV inclination-matched age models (Steen, 2016), but focus here on the more likely version (PSV-1). It was constructed from 14 tie points selected by visual wiggle-matching of the prominent features in the Cascade

335 Lake inclination record with CALS10k.1b (9 tie points), pfm9k.1b (8 tie points), and the Burial Lake records (9 tie points) (Fig. 9; Table 3). Not all tie points are present in all records due to the limited age of the CALS10k.1b and pfm9k.1b models (10 ka and 9 ka, respectively) and limited prominent features in the upper part of the Burial Lake record. The depths of all tie points and their age uncertainties were fit with a smooth spline using CLAM software to generate the Cascade Lake PSV-1 age model (Fig. 10). Where the ages of tie points from Burial Lake are somewhat older than those from the field models,

340 between about 270 and 170 cm, the PSV-1 age modeled more closely follows the field models because it is based on a higher density of control points.

The PSV-1 age model and the radiometric age model overlap within their uncertainties from the base of the radiometrically dated section, at around 365 cm, up to around 160 cm (between ~ 16 and 6 ka) (Fig. 10). The PSV-1 age model can be extended beyond the radiometric age model to ~ 21 ka using the tie points between the Cascade Lake inclination record (CASC-4A-2D

345 depth scale) correlated with the similar record at Burial Lake (Dorfman 2013), although the radiocarbon age-depth model for this portion of the Burial Lake sediment core is not well constrained. Above around 160 cm depth (~ 6 ka), the ages of fluctuations in Cascade Lake begin to diverge from those of the regional records, reaching a maximum offset of around 2000 y at around 4 ka, and then decreasing towards the present.

Table 3. Paleomagnetic inclination tie points used to develop Cascade Lake age model PSV-1.

Tie point*	Cascade Lake composite depth blf (cm)	Burial Lake Age (a BP)	Burial Lake uncertainty (± a)[#]
1	60	2272	486
2	80	2753	302
3	155	4808	529
4	177	7276	138
5	189	-	-
6	203	-	-
7	228	9878	407
8	246	-	-
9	284	11937	495
10	357	15455	705
11	419	17056	386
12	427	17414	551
13	454	18130	785
14	509	20518	1131

* Tie points shown in Figure 9.
[#] One half of 1 sigma range.
[§] Assumed age uncertainty of ± 500 years.

350
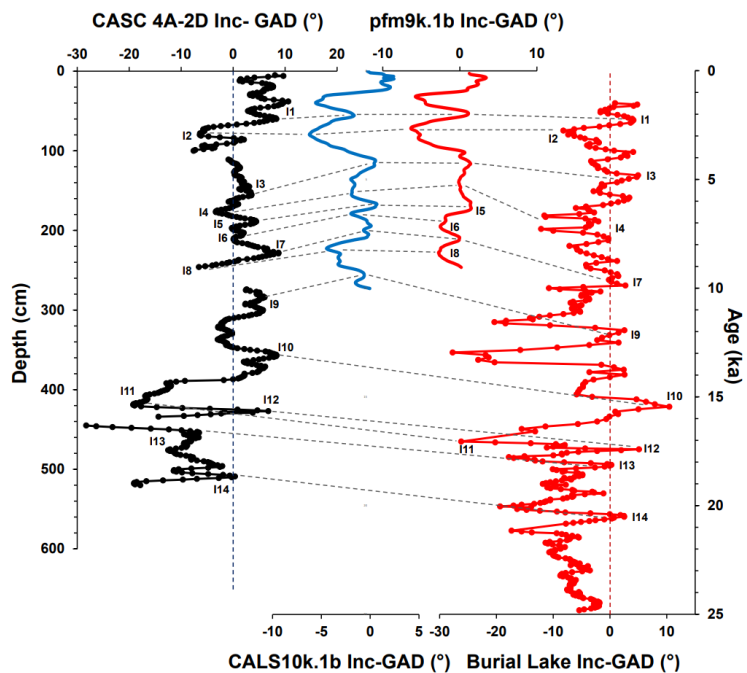
Figure 9: Cascade Lake PSV-1 inclination age control points using the CALS10k.1b (Korte et al., 2011) and pfm9k.1b (Nilsson et al., 2014) field models and the Burial Lake inclination record (Dorfman, 2013). Tie-point ages are listed in Table 3.
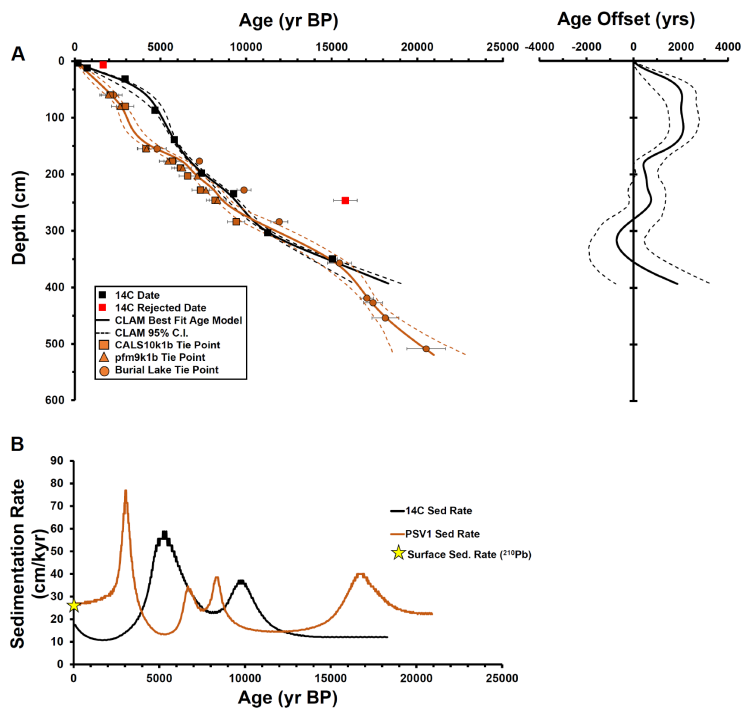
Figure 10: Cascade Lake radiometric-based age model and 95% C.I. (black) (Fig. 8) compared with the paleomagnetic secular variation (PSV-1) age model and 95% C.I. (orange).

355

5.3 Age model discrepancies

The disagreement between the PSV-1 and the radiometric age models may arise for multiple reasons. First, the three ^{14}C dates
360 between 140 and 30 cm might be too old. Because the surrounding bedrock includes limestone and dolomite of the Pennsylvanian-Mississippian Lisburne Group (Mull et al., 1994), a hard-water effect is likely operating within the lake, resulting in artificially old ^{14}C dates. Hard-water effects are known from many lakes; for example, they are responsible for age offsets of several hundred years in the Great Lakes (e.g., Rea and Colman, 1995; Moore et al., 1998). Due to a lack of sufficient terrestrial macrofossil material, all dated ^{14}C samples from Cascade Lake contained some component of aquatic organic
365 material (Table 2) that likely incorporated bicarbonate with no radiocarbon. Alternatively, ^{14}C dates may be too old due to terrestrial "old carbon" being washed into the lake from organic matter stored within the watershed. Gaglioti et al. (2014) demonstrate that a significant amount of ancient organic carbon was incorporated into sediments of another lake (Lake of the Pleistocene) in the region during the late glacial and Holocene, especially during intervals when permafrost thaw thickened the active layer.

370 Some of the age offset might be explained by a post-depositional remanent magnetization (pDRM) lock-in effect, where the acquisition of the magnetization occurs below the sediment water interface (Irving and Major, 1964). PSV records from organic-rich varved lake sediments in Sweden matched reference curves best when accounting for lock-in depths of 21–34 cm (Mellström et al., 2015; Snowball et al., 2013). Using differences between floating varve chronologies and ^{14}C wiggle-matched chronologies, Mellström et al. (2015) suggested that complete lock-in may not be achieved until 50–160 cm at Gyltigesjön
375 and 30–80 cm at Kälksjön (west-central Sweden) in sediment with high organic-matter content and low bulk density. If a similarly pronounced pDRM lock-in depth was a feature of the Cascade Lake sediment, then the radiometric age model could be closer to correct.

Importantly, however, new cryptotephra analyses (Davies et al., this issue) from the same core analyzed for magnetic properties (CASC-4A) identified tephras whose ages support the PSV-1 age model as well as our conclusion that the pDRM lock-in
380 depth is not significant in Cascade Lake (Fig. 10). Specifically, tephras in the upper 1.1 m of sediment have been geochemically correlated with eruptions of Opala (~1400 cal BP), Mt. Churchill (~1700 cal BP), Ruppert tephra (~2450 cal BP) and Aniakchak (~3500 cal BP). These correlated tephra ages provide strong evidence for a ^{14}C age offset due to a hard-water effect or remobilization of old carbon in the watershed after around 6 ka, with this effect reaching a peak around 4 ka. Because the ^{14}C samples contain a mixture of aquatic and terrestrial materials (Table 2), which was necessary to obtain sufficient mass for
385 conventional AMS ^{14}C techniques, it is not possible to investigate the extent to which the old carbon signal is carried by aquatic versus the terrestrial components.

5.4 Comparison with regional records of geomagnetic field variability

Inclination, declination and RPI variability for the past ~ 21 kyr at Cascade Lake can be compared with other regional Alaskan, western North American, and Arctic records during the late Pleistocene and Holocene (Fig. 11). Previous published records
390 include Burial Lake (Dorfman, 2013), core 85JC, Gulf of Alaska (Walczak et al., 2017) core 8JPC, Chukchi Sea (Lisé-Pronovost et al., 2009), Grandfather Lake, southwest Alaska (Geiss and Banerjee, 2003), and core 803, Beaufort Sea (Barletta et al., 2008). Comparisons with the lower part of the sequence (unit L1 and L2, > 16 ka) should be treated with caution as magnetic mineralogy with low S-ratios, implying a large percentage of hematite, while lower ARM and k_{ARM}/k suggest little magnetite and what is there is likely to be coarser grained (Fig 3 and 4), along with higher MAD values (Fig. 5) all imply a
395 lithology less suited for geomagnetic reconstruction. in those intervals are not optimal for recording the geomagnetic field.

Similar inclination features can be identified in individual records, including core 85JC and Grandfather Lake (not incorporated in CALS10k.1b or pfm9k.1b) (Fig. 11a). Notably, the timing of low inclination at Cascade Lake around 2.8 ka is similar to

that at Grandfather Lake (~ 2.4 ka), core 803 (~ 2.5 ka), and core 8JPC (~ 2.9 ka). This pervasive feature may be related to a significant eastward swing in declination that is observed in northern Europe at ~ 2.8–2.5 ka, described as the "f-event" (e.g.,

400 Turner and Thompson, 1981; Snowball and Sandgren, 2002; 2004). There is evidence that centennial- and millennial-scale PSV and intensity features in North America and Europe are often out of phase during the Holocene (Stoner et al., 2013), possibly resulting from an oscillating "eccentric dipole" field behavior (e.g., Gallet et al., 2009), with alternating periods when geomagnetic flux patches centered over either North America or Europe are dominant. Therefore, an "archeomagnetic jerk" such as the "f-event" (Gallet et al., 2009), identified as an eastward declination swing in North Atlantic PSV records, may be

405 recorded as an inclination low in parts of North America because of growth of flux over European shifted toward an intensity high (Stoner et al., 2013; Walczak et al., 2017). Though the timing of this North American inclination low is broadly contemporaneous with the European "f-event", a deeper understanding of spatial geomagnetic field behavior and better chronological control is required to confirm that these events are correlative.

Additionally, rapid, high-amplitude inclination and declination changes occurring around 18–17 ka in Cascade Lake are not

410 associated with shifts in sediment type in unit L1, and they are replicated in the Burial Lake and 85JC records (Fig. 11a, b). The occurrence of a possible geomagnetic excursion has been documented at ~ 17 ka builds upon previous knowledge of low inclination around ~ 18–17 ka in the western U.S. (Rieck et al., 1992; Liddicoat and Coe, 2011; Turrin et al., 2013). Transformation of Cascade Lake component directions to virtual geomagnetic poles (VGPs) yields a minimum VGP latitude of 51.2° N, which is a 38.8° displacement from the geographic north pole. High-amplitude inclination shifts at this time are

415 contemporaneous with low relatively paleointensity estimates (Fig. 11) and elevated MAD values (Fig. 5) that might be expected during excursions, which usually exhibit low geomagnetic field intensity (e.g., Laj and Channell, 2007; Channell, 2014). More documentation of geomagnetic field behavior during this interval, especially at high latitudes, is necessary to positively correlate the ~ 17 ka excursion documented elsewhere with rapid inclination shifts in the Cascade Lake, Burial Lake, and 85JC records.

420 **5.5 Relative paleointensity**

The mechanism by which the past intensity of the geomagnetic field is preserved in sediments is not completely understood (Roberts et al., 2013). Therefore, to infer RPI, a series of quality assessment requirements must be met. A comprehensive review of RPI studies (Tauxe, 1993, and references therein) outlines some prerequisites for developing meaningful paleointensity estimates: (1) the dominant magnetic mineral should be magnetite in the grain-size range of 1-15 μm; (2) the

425 ChRM of the magnetite should display a stable, well-defined vector component; (3) depositional remanent magnetization (DRM) must accurately record the geomagnetic field, and there should be minimal discrepancy between inclination of the ChRM and that of the expected GAD for the site latitude; (4) down-core concentrations of magnetic minerals should not vary by more than an order of magnitude; (5) the ChRM should be normalized by multiple methods (e.g., k_{LF}, IRM, ARM) with similar results; and (6) RPI should not correlate strongly with rock magnetic parameters of sediment (e.g., ARM, IRM,

430 susceptibility, coercivity). Stoner and St-Onge (2007) add to these criteria, recommending that: (1) all samples should be subjected to alternating field (AF) demagnetization to reveal component magnetization and high- and low-coercivity components; and (2) ChRM MAD values should be no more than 5° for RPI studies.

Unit L3 appears to meet most of the criteria for RPI studies, as evidenced by inclination relative to expected GAD inclination (Fig. 5), remarkably low MAD values (Fig. 5), and stable demagnetization behavior (Fig. 6). Magnetic grain-size estimation

435 (Fig. 3 and 4) suggests fine PSD magnetite, while SD magnetite can be a very efficient paleomagnetic recorder, even when it is of biogenic origin (Roberts et al., 2011).
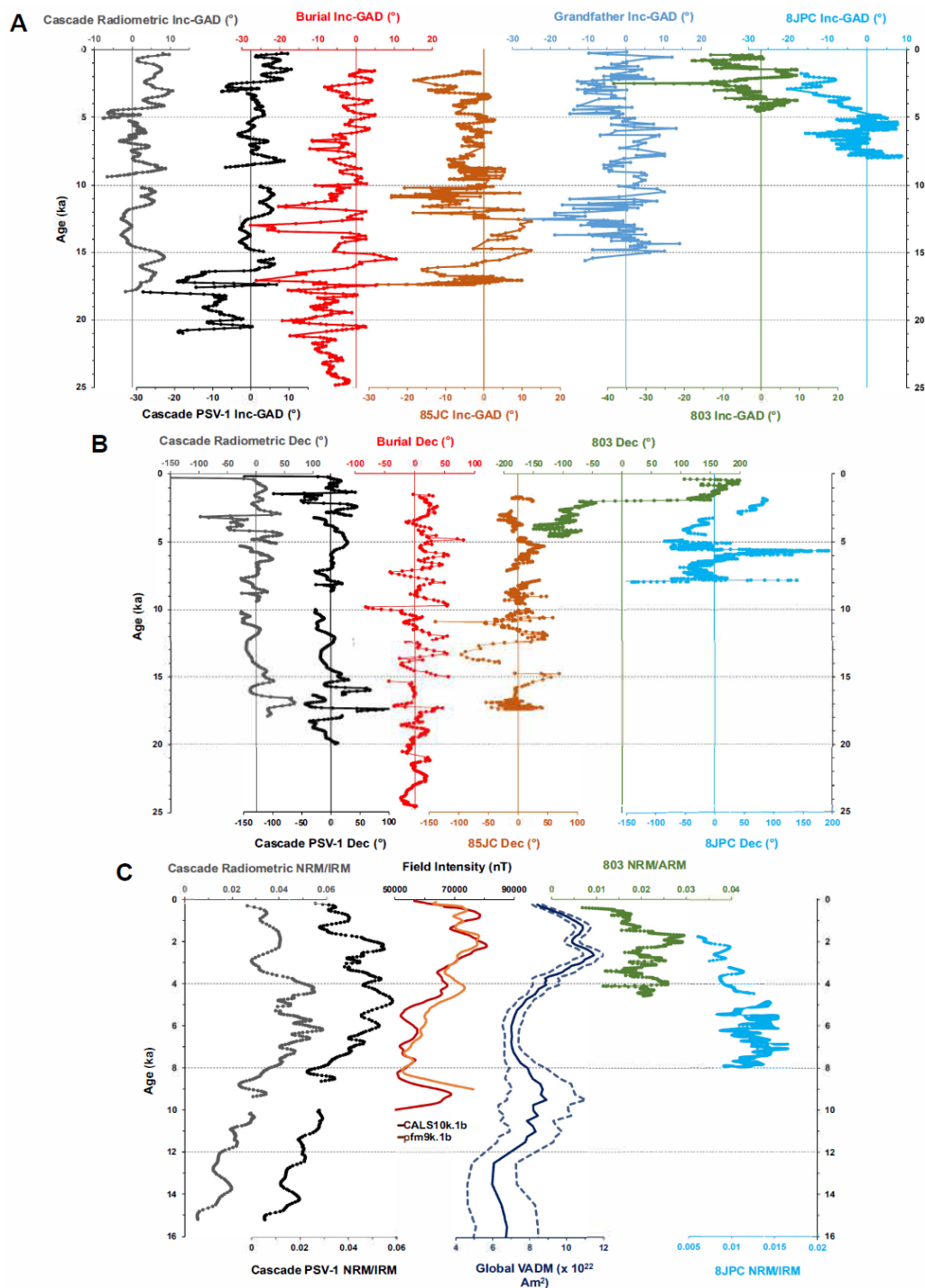
Figure 11: Cascade Lake paleomagnetic record compared with regional and global records. (**A**) Paleomagnetic inclination relative to geocentric axial dipole (GAD) predictions. (**B**) Paleomagnetic declination. (**C**) NRM/IRM compared with regional and global geomagnetic intensity estimates and regional relative paleo intensity records. Included are Burial Lake, Brooks Range, Alaska (Dorfman, 2013), core 85JC, Gulf of Alaska (Walczak et al., 2017), Grandfather Lake, southwest Alaska (Geiss and Banerjee, 2003), core 803, Beaufort Sea (Barletta et al., 2008), and core 8JPC, Chukchi Sea (Lisé-Pronovost et al., 2009). Paleointensity estimates are provided for the CALS10k.1b (Korte et al., 2011) and pfm9k.1b (Nilsson et al., 2014) geomagnetic field models and the global virtual axial dipole moment (VADM) reconstruction of Knudsen et al. (2008).

We propose that, based on high R-values, minimal resemblance to the normalizer, and general agreement with various normalization methods, $NRM_{20-70mT}/IRM_{20-70mT}$ is the best selection for an RPI proxy for the Cascade Lake record. Due to the rapid lithologic change and significantly lower normalized remanence estimates in L2, we suggest that RPI estimates for this interval are unreliable, as lithologic variability has possibly not been adequately removed.

450 RPI estimates for Cascade Lake ($NRM_{20-70mT}/IRM_{20-70mT}$) for the past ~10 kyr are similar to core 803 NRM/ARM and with field strength estimates from CALS10k.1b and pfm9k.1b over the last few thousand years (Fig. 11c). Specifically, RPI peaks at ~ 4.8, 2.3, and 0.9 ka are persistent regional features, though CALS10k.1b and pfm9k.1b display an earlier mid-Holocene RPI peak at 4.4–4.2 ka. But the general shapes of the curves are quite different, especially prior to 4 ka, with higher values than the spherical harmonic models predict. This is partially supported by 8JPC that also shows generally higher intensity

455 during this time interval. Estimates of Cascade Lake RPI earlier than 10 ka should be treated with caution until additional late Pleistocene and Holocene paleointensity records become available from this region.

6 Conclusions

Paleomagnetic data from Cascade Lake sediment add to our knowledge of geomagnetic field variability in the Arctic back to 21 ka. RPI reconstructions over the past 15 ka, especially the $NRM_{20-70mT}/IRM_{20-70mT}$ proxy, are promising and compare well

460 with regional records. However, similarities with ARM concentrations suggest that the record should be treated with caution because the implied higher-than-expected intensities during the mid-Holocene, if supported through replication, would have significant geomagnetic implications.

The paleomagnetic data also extend and improve the radiometric-based age model from Cascade Lake. Prominent features (tie points) in the Cascade Lake paleomagnetic inclination record can be wiggle-matched with similar features in two geomagnetic

465 field models (Korte et al., 2011; Nilsson et al., 2014) and in the inclination record from Burial Lake (Dorfman, 2013). Tie points can be correlated between Cascade and Burial Lakes to extend the age model at Cascade Lake below the lowest ^{14}C age at 15 ka, back to 21 ka. Tie-point ages diverge from the radiometric-based ages in the upper 1.6 m of the sediment, by up to about 2000 years at around 4 ka. The recent discovery of four identifiable late Holocene cryptotephra in this section of the core (Davis et al., this issue) supports the PSV chronology and suggests that hard water or aged organic material is a likely

470 explanation for the age offset. In a companion study, Davies et al. (this issue) integrate the PSV age model with corroborating evidence based on ^{14}C, ^{210}Pb, and cryptotephra, in a Bayesian framework to generate the best estimate for the age-depth relation. This firm geochronological footing increases the value of the Cascade Lake sedimentary sequence as an archive for future paleoenvironmental and paleoclimatologic studies.

475 **Data availability** The down-core data for the multi-parameter properties analyzed on the sediment cores from Cascade Lake, including all data used to plot the figures in this article, are in an Excel workbook file as one of the resources available with this online publication.

Author contribution DPS conducted the analyses, wrote the initial draft and curated the data. JSS validated the interpretations
480 and provided training and laboratory resources. JPB co-led and co-funded the project. DSK conceptualized, co-led and co-funded the study. All co-authors provided critical reviews and revisions.
Competing interests The authors declare that they have no conflict of interest.

Acknowledgments We thank D. Fortin and E. Ceperley for assistance with lake coring, LacCore and the Institute of Rock
485 Magnetism (University of Minnesota) for assistance with core processing and hysteresis measurements, Flett Research for ^{210}Pb measurements, and Keck Carbon Cycle AMS Lab (UC Irvine) for ^{14}C analyses. We also thank F. Barletta, C. Geiss, and

A. Lisé-Pronovost for sharing paleomagnetic data, B. Reilly and the P-Mag Lab (Oregon State University) group for helpful data discussions.

490 **Financial support** This research was supported by the National Science Foundation grants #1107662 (DSK) and #1107854 (JPB), and awards from Pioneer Natural Resources and the Geological Society of America (DPS).

References

Amit, H., Aubert, J., and Hulot, G.: Stationary, oscillating, or drifting mantle-driven geomagnetic flux patches?, J. Geophys. Res., 115, B07108, doi:1029/2009JB006542, 2010.

495 Appleby, P.G., and Oldfield, F.: The calculation of lead-210 dates assuming a constant rate of supply of unsupported ^{210}Pb to the sediment, Catena, 5, 1-8, doi:10.1016/S0341-8162(78)80002-2, 1978.

Aurnou, J., Andreadis, S., Zhu, L., and Olson, P.: Experiments on convection in Earth's core tangent cylinder, Earth Planet. Sci. Lett., 212, 119-134, doi:10.1016/S0012-821X(03)00237-1, 2003.

Barletta, F., St-Onge, G., Channell, J.E.T., Rochon, A., Polyak, L., and Darby, D.: High-resolution paleomagnetic secular

500 variation and relative paleointensity records from the western Canadian Arctic: implication for Holocene stratigraphy and geomagnetic field behaviour, Can. J. Earth Sci., 45, 1265-1281, doi:10.1139/E08-039, 2008.

Barletta, F., St-Onge, G., Channell, J.E.T., and Rochon, A.: Dating of Holocene western Canadian Arctic sediments by matching paleomagnetic secular variation to a geomagnetic field model, Quat. Sci. Rev., 29, 2315-2324, doi:10.1016/j.quascirev.2010.05.035, 2010.

505 Binford, M.W.: Calculation and uncertainty analysis of 210Pb dates for PIRLA project lake sediment cores, J. Paleolimnol., 3, 253-267, doi:10.1007/BF00219461, 1990.

Blaauw, M.: Methods and code for 'classical' age-modelling of radiocarbon sequences, Quat. Geochron., 5, 512-518, doi:10.1016/j.quageo.2010.01.002, 2010.

Bloxham, J., and Gubbins, D.: Thermal core-mantle interactions, Nature, 325, 511-513, doi:10.1038/325511a0, 1987.

510 Bloxham, J., Gubbins, D., and Jackson, A.: Geomagnetic secular variation, Philos. Trans. R. Soc. Lon., 329, 415-502, doi:10.1098/rsta.1989.0087, 1989.

Channell, J.E.T.: The Iceland Basin excursion: Age, duration, and excursion field geometry, Geochem. Geophys. Geosyst., 15, 4920-4935, doi:10.1002/2014GC005564, 2014.

Channell, J.E.T., Mazaud, A., Sullivan, P., Turner, S., and Raymo, M.E.: Geomagnetic excursions and paleointensities in the

515 Matuyama Chron at Ocean Drilling Program Sites 983 and 984 (Iceland Basin), J. Geophys. Res., 107, B62114, doi:10.1029/2001JB000491, 2002.

Channell, J.E.T., and Guyodo, Y.: The Matuyama Chronozone at ODP Site 982 (Rockall Bank): Evidence for Decimeter-Scale Magnetization Lock-in Depths, in Timescales of the Paleomagnetic Field, Geophys. Monogr., vol. 145, edited by J. E. T. Channell et al., AGU, Washington, D. C, 2004.

520 Cox, A.: Latitude dependence of the angular dispersion of the geomagnetic field, Geophys. J. R. Astron. Soc., 20, 253-269, doi:10.1111/j.1365-246X.1970.tb06069.x, 1970.

Davies, L.J., Jensen, B.J.L., Kaufman, D.S. (in review) Late Holocene cryptotephra and Bayesian age model for the 21,000 year sedimentary sequence from Cascade Lake, Alaska, Geochronology, this issue.

Day, R., Fuller, M., and Schmidt, V.A.: Hysteresis properties of titanomagnetites: grain-size and compositional dependence,

525 Phys. Earth Planet. Int., 13, 260-267, doi:10.1016/0031-9201(77)90108-X, 1977.

Donadini, F., Korhonen, K., Riisager, P., and Pesonen, L.J.: Database for Holocene geomagnetic intensity information, EOS: Trans. Am. Geophys. Un., 87, 137-138, doi:10.1029/2006EO140002, 2006.

Donadini, F., Korte, M., and Constable, C.: Geomagnetic field for 0-3 ka: 1. New data sets for global modeling, Geochem. Geophys. Geosyst., 10, doi:10.1029/2008GC002295, 2009.

530 Dorfman, J.M.: A 37,000-year record of Paleomagnetic Secular Variation from Burial Lake, Arctic Alaska, M.S. thesis, Oregon State University, 2013.

Dorfman, J.M., Stoner, J.S., Finkenbinder, M.S., Abbott, M.B., Xuan, C., and St-Onge, G.: A 37,000-year environmental record of aeolian dust deposition from Burial Lake, Arctic Alaska, Quat. Sci. Rev., 128, 81-97, doi:10.1016/j.quascirev.2015.08.018, 2015.

535 Fabian, K., and von Dobeneck, T.: Isothermal magnetization of samples with stable Preisach function: A survey of hysteresis, remanence, and rock magnetic parameters, J. Geophys. Res., 102(B8), 17659–17677, doi:10.1029/97JB01051, 1997.

Finkenbinder, M.S., Abbott, M.B., Stoner, J.S., and Dorfman, J.M.: A multi-proxy reconstruction of environmental change spanning the last 37,000 years from Burial Lake, Arctic Alaska, Quat. Sci. Rev., 126, 227-241,doi: 10.1016/j.quascirev.2015.08.031, 2015.

540 Gaglioti, B.V., Mann, D.H., Jones, B.M., Pohlman, J.W., Kunz, M.L., and Wooller, M.J.: Radiocarbon age-offsets in an arctic lake reveal the long-term response of permafrost carbon to climate change, J. Geophys. Res. Biogeosci., 119, 1630–1651, doi:10.1002/2014JG002688, 2014.

Gallet, Y., Hulot, G., Chulliat, A., and Genevey A.: Geomagnetic field hemispheric asymmetry and archeomagnetic jerks, Earth Planet. Sci. Lett., 284, 179-186, doi:10.1016/j.epsl.2009.04.028, 2009.

545 Geiss, C.E., and Banerjee, S.K.: A Holocene-Late Pleistocene geomagnetic inclination record from Grandfather Lake, SW Alaska, Geophys. J. Int., 153, 497-507, doi:10.1046/j.1365-246X.2003.01921.x, 2003.

Hamilton, T.D.: Surficial geologic map of the Killik River Quadrangle, Alaska, U.S. Geological Survey Miscellaneous Field Studies Map 1234, 1 sheet, scale 1:250,000, 1980.

Hamilton, T.D.: Quaternary stratigraphic sections with radiocarbon dates, Killik River Quadrangle, Alaska, U.S. Geological
550 Survey Open File Report, 82-606, 1982.

Irving, E. and Major, A.: Post-depositional detrital remanent magnetization in a synthetic sediment, Sedimentology, 3, 135–143. doi:10.1111/j.1365-3091.1964.tb00638.x, 1964.

King, J., Banerjee, S.K., Marvin, J., and Özdemir, Ö.: A comparison of different magnetic methods for determining the relative grain size of magnetite in natural materials: some results from lake sediments. Earth Planet. Sci. Lett., 59, 404-419, 1982.

555 Kirschvink, J.L.: The least-squares line and plane and the analysis of paleomagnetic data, Geophys. J. Int., 62, 699-718, doi:10.1111/j.1365-246X.1980.tb02601.x, 1980.

Knudsen, M.F., Riisager, P., Donadini, F., Snowball, I., Muscheler, R., Korhonen, K., and Pesonen, L.J.: Variations in the geomagnetic dipole moment during the Holocene and the past 50 kyr, Earth Planet. Sci. Lett., 272, 319-329, doi:10.1016/j.epsl.2008.04.048, 2008.

560 Korhonen, K., Donadini, F., Riisager, P., and Pesonen, L.J.: GEOMAGIA50: An archeointensity database with PHP and MySQL, Geochem. Geophys. Geosyst., 9, doi:10.1029/2007GC001893, 2008.

Korte, M., and Holme, R.: On the persistence of geomagnetic flux lobes in global Holocene field models, Phys. Earth Planet. Int., 182, 179-186, doi:10.1016/j.pepi.2010.08.006, 2010.

Korte, M., Constable, C., Donadini, F., and Holme, R.: Reconstructing the Holocene geomagnetic field, Earth Planet. Sci.
565 Lett., 312, 497-505, doi:10.1016/j.epsl.2011.10.031, 2011.

Laj, C., and Channell, J.E.T.: Geomagnetic Excursions, Treatise on Geophysics, 5, 373-416, doi:10.1016/B978-044452748-6.00095-X, 2007.

Liddicoat, J.C., and Coe, R.S.: Possible recording of the Hilina Pali excursion in the Mono Basin, California, Geol. Soc. Am. Abst. Progr., 43, 512, 2011.

570 Lisé-Pronovost, A., St-Onge, G., Brachfeld, S., Barletta, F., and Darby, D.: Paleomagnetic constraints on the Holocene stratigraphy of the Arctic Alaskan margin, Global Planet. Change, 68, 85-99, doi:10.1016/j.gloplacha.2009.03.015, 2009.

Lowe, J.J., Ramsey, C.B., Housley, R.A., et al.: The RESET project: Constructing a European tephra lattice for refined synchronisation of environmental and archaeological events during the last c. 100 ka. Quat. Sci. Rev., 118, 1–17, doi:10.1016/j.quascirev.2015.04.006, 2015.

575 Lurcock, P.C., and Wilson, G.S.: PuffinPlot: A versatile, user-friendly program for paleomagnetic analysis, Geochem. Geophys. Geosyst., 13, Q06Z45, doi:10.1029/2012GC004098, 2012.

Mellström, A., Nilsson, A., Stanton, T., Muscheler, R., Snowball, I., and Suttie, N.: Post-depositional remanent magnetization lock-in depth in precisely dated varved sediments assessed by archaeomagnetic field models, Earth Planet. Sci. Lett., 410, 186-196, doi:10.1016/j.epsl.2014.11.016, 2015.

580 Moore, Jr., T.C., Rea, D.K., and Godsey, H.: Regional variation in modern radiocarbon ages and the hard-water effects in Lake Michigan and Huron. J. Paleolimnol., 20, 347-351, doi:10.1023/A:1007920723163, 1998.

Mull, C.G., Moore, T.E., Harris, E.E., and Tailleur, I.L.: Geologic map of the Killik River Quadrangle, Brooks Range, Alaska, U.S. Geological Survey Open-File Report 94-679, 1 sheet, scale 1:125,000, 1994.

Nilsson, A., Holme, R., Korte, M., Suttie, N., and Hill, M.: Reconstructing Holocene geomagnetic field variation: new 585 methods, models, and implications, Geophys. J. Int., 198, 229-248, doi:10.1093/gji/ggu120, 2014.

Oda, H., and Xuan, C.: Deconvolution of continuous paleomagnetic data from pass-through magnetometer: A new algorithm to restore geomagnetic and environmental information based on realistic optimization, Geochem. Geophys. Geosyst., 15, 3907-3924, doi:10.1002/2014GC005513, 2014.

Ólafsdóttir, S., Geirsdóttir, À., Miller, G.H., Stoner, J.S., and Channell, J.E.T.: Synchronizing Holocene lacustrine and marine 590 sediment records using paleomagnetic secular variation, Geology, 41, 535-538, doi:10.1130/G33946.1, 2013.

Ólafsdóttir, S., Reilly, B.T., Bakke, J., Stoner, J.S., Gjerde, M., and van der Bilt, W.G.M.: Holocene paleomagnetic secular variation (PSV) near 80 degrees N, Northwest Spitsbergen, Svalbard: Implications for evaluating High Arctic sediment chronologies. Quat. Sci. Rev., 210, 90-102, doi: 10.1016/j.quascirev.2019.03.003, 2019.

Rea, D.K., and Colman, S.M.: Radiocarbon ages of pre-bomb clams and the hard-water effect in Lakes Michigan and Huron, 595 J. Paleolimnol., 14, 89-91, doi:10.1007/BF00682596, 1995.

Reimer, P.J., Bard, E., Bayliss, A., Beck, J.W., Blackwell, P.G., Bronk Ramsey, C., Buck, C.E., Cheng, H., Edwards, R.L., Friedrich, M., Grootes, P.M., Guilderson, T.P., Haflidason, H., Hajdas, I., Hatté, C., Heaton, T.J., Hoffmann, D.L., Hogg, A.G., Hughen, K.A., Kaiser, K.F., Kromer, B., Manning, S.W., Niu, M., Reimer, R.W., Richards, D.A., Scott, E.M., Southon, J.R., Staff, R.A., Turney, C.S.M., and van der Plicht, J.: IntCal13 and Marine13 radiocarbon age calibration 600 curves 0–50,000 years cal BP, Radiocarbon, 55, 1869–1887, doi:10.2458/azu_js_rc.55.16947, 2013.

Rieck, H.J., Sarna-Wojcicki, A.M., Meyer, C.E., and Adam, D.P.: Magnetostratigraphy and tephrochronology of an upper Pliocene to Holocene record in lake sediments and Tulelake, northern California, Geol. Soc. Am. Bull., 104, 409-428, doi:10.1130/0016-7606(1992)104<0409:MATOAU>2.3.CO;2, 1992.

Roberts, A.P., Cui, Y., and Verosub, K.L.: Wasp-waisted hysteresis loops: Mineral magnetic characteristics and discrimination 605 of components in mixed magnetic systems, J. Geophys. Res., 100, 17909-17924, doi:10.1029/95JB00672, 1995.

Roberts, A.P., Florindo, F., Villa, G., Chang, L., Jovane, L., Bohaty, S.M., Larrasoaña, J.C., Heslop, D. and Fitz Gerald, J.D.: Magnetotactic bacterial abundance in pelagic marine environments is limited by organic carbon flux and availability of dissolved iron, Earth Planet. Sci. Lett., 310, 441-452, doi:10.1016/j.epsl.2011.08.011, 2011.

Roberts, A.P., Tauxe, L., and Heslop, D.: Magnetic paleointensity stratigraphy and high-resolution Quaternary geochronology: 610 successes and future challenges, Quat. Sci. Rev., 61, 1-16, doi:10.1016/j.quascirev.2012.10.036, 2013.

Roberts, A.P., Tauxe, L., Heslop, D., Zhao, X., and Jiang, Z.: A critical appraisal of the "Day" diagram. J. Geophys. Res.: Solid Earth, 123, 2618–2644. doi:10.1002/2017JB015247, 2018.

Snowball, I., and Sandgren, P.: Geomagnetic field variations in northern Sweden during the Holocene quantified from varved lake sediments and their implications for cosmogenic nuclide production rates, Holocene, 12, 517-530, doi:10.1191/0959683602hl562rp, 2002.

Snowball, I., and Sandgren, P.: Geomagnetic field intensity changes in Sweden between 9000 and 450 cal BP: extending the record of "archaeomagnetic jerks" by means of lake sediments and the pseudo-Thellier technique, Earth Planet. Sci. Lett., 227, 361-376, doi:10.1016/j.epsl.2004.09.017, 2004.

Snowball, I., Mellström, A., Ahlstrand, E., Haltia, E., Nilsson, A., Ning, W., Muscheler, R., and Brauer, A.: An estimate of post-depositional remanent magnetization lock-in depth in organic rich varved lake sediments, Global Planet. Change, 110, 264-277, doi:10.1016/j.gloplacha.2013.10.005, 2013.

Steen, D.P.: Late Quaternary paleomagnetism and environmental magnetism at Cascade and Shainin Lakes, north-central Brooks Range, Alaska, MS Thesis, Northern Arizona University, ProQuest 10126253, 2016.

Stoner, J.S., and St-Onge, G.: Chapter Three: Magnetic Stratigraphy in Paleoceanography: Reversals, Excursions, Paleointensity, and Secular Variation, Developments in Marine Geology, 1, 99-138, doi:10.1016/S1572-5480(07)01008-1, 2007.

Stoner, J.S., Jennings, A., Kristjánsdóttir, G.B., Dunhill, G., Andrews, J.T., and Harardóttir, J.: A paleomagnetic approach toward refining Holocene radiocarbon-based chronologies: Paleoceanographic records from the north Iceland (MD99-2269) and east Greenland (MD99-2322) margins, Paleoceanography, 22, PA1209, doi:10.1029/2006PA001285, 2007.

Stoner, J.S., Channell, J.E.T., Mazaud, A., Strano, S.E., and Xuan, C.: The influence of high-latitude flux lobes on the Holocene paleomagnetic record of IODP Site U1305 and the northern North Atlantic, Geochem. Geophys. Geosyst., 14, 4623-4646, doi:10.1002/ggge.20272, 2013.

St-Onge, G., and Stoner, J.S.: Paleomagnetism near the north magnetic Pole: a unique vantage point for understanding the dynamics of the geomagnetic field and its secular variations. Oceanography 24, 42e50. doi:10.5670/oceanog. 2011.53, 2011.

Stuiver, M., Reimer, P.J., and Reimer, R.W.: CALIB 5.0. (http://www.calib.qub.ac.uk/calib/), 2005.

Tauxe, L.: Sedimentary records of relative paleointensity of the geomagnetic field: theory and practice, Rev. Geophys., 31, 319-354, doi:10.1029/93RG01771, 1993.

Tauxe, L., Mullender, T.A.T., and Pick, T.: Potbellies, wasp-waists, and superparamagnetism in magnetic hysteresis, J. Geophys. Res., 101, 571-583, doi:10.1029/95JB03041, 1996.

Turner, G.M., and Thompson, R.: Lake sediment record of the geomagnetic secular variation in Britain during Holocene times, Geophys. J. R. Astron. Soc., 65, 703-725, doi:10.1111/j.1365-246X.1981.tb04879, 1981.

Turrin, B.D., Champion, D.E., Mortlock, R.A., Fairbanks, R.G., and Swisher, C.C.: ^{40}Ar/^{39}Ar and U-series ages of Late Pleistocene geomagnetic excursion in Western North America: The Hilina Pali event in Western North America, Am. Geophys. Un. Fall Meet. Abst. Progr., GP31A-06, 2013.

Walczak, M.H., Stoner, J.S., Mix, A.C., Jaeger, J., Rosen, G.P., Channell, J.E.T., Heslop, D., and Xuan, C.: A 17,000 yr paleomagnetic secular variation record from the southeast Alaskan margin: Regional and global correlations, Earth Planet. Sci. Lett., 473, 177-189, doi:10.1016/j.epsl.2017.05.022, 2017.

Wang, D., and Van der Voo, R.: The hysteresis properties of multidomain magnetite and titanomagnetite/titanomaghemite in mid-ocean ridge basalts, Earth Planet. Sci. Lett., 220, 175-184, doi:10.1016/S0012-821X(04)00052-4, 2004.

Xuan, C., and Channell, J.E.T.: UPmag: software for viewing and processing u channel and other pass-through paleomagnetic data, Geochem. Geophys. Geosyst., 10, Q10Y07, doi:10.1029/2009GC002584, 2009.